



ELSEVIER

Available online at www.sciencedirect.com

SCIENCE @ DIRECT®

Global and Planetary Change 49 (2005) 75–93

GLOBAL AND PLANETARY
CHANGE

www.elsevier.com/locate/gloplacha

Mid-Holocene strengthening of the Southern Westerlies in South America — Sedimentological evidences from Lago Cardiel, Argentina (49°S)

Adrian Gilli ^{a,*}, Daniel Ariztegui ^b, Flavio S. Anselmetti ^a, Judith A. McKenzie ^a, Vera Markgraf ^c, Irka Hajdas ^d, Robert D. McCulloch ^e

^aGeological Institute, Swiss Federal Institute of Technology ETHZ, Sonneggstrasse 5, 8092 Zürich, Switzerland

^bInstitute F.A. Forel and Department of Geology and Paleontology, University of Geneva, Rue des Maraichers 13, 1205 Geneva, Switzerland

^cInstitute of Arctic and Alpine Research, University of Colorado, Boulder, CO 80309-0450, USA

^dPSI/ETH AMS ¹⁴C Laboratory Höggerberg, HPK, 8093 Zürich, Switzerland

^eSchool of Biological and Environmental Sciences, University of Stirling, Stirling FK9 4LA, UK

Received 28 September 2004; accepted 28 May 2005

Abstract

The paleoclimatic evolution of southern South America is characterized to a large extent by the behavior (strength and latitudinal position) of the storm tracks of the Southern Westerlies. Our study site, Lago Cardiel (49°S), lies within the modern influence of the Southern Westerlies and, therefore, is ideally located to track the past migrations of these storm tracks. With a coring strategy taking into account the lateral differences in sedimentation and an excellent core-to-core correlation using tephra layers, a composite sedimentological record of almost 25 m was established covering the last ~16,000 cal yr. Sedimentological and petrophysical analysis of the cores revealed the establishment of a dominant lake current since 6800 cal yr BP leading to a drift deposition, which is especially well-expressed in the sedimentary record by an increase in magnetic susceptibility values. As this pattern of currents is most likely induced by wind activity, we propose that the observed increase in magnetic susceptibility documents an intensification of the westerly storm tracks. This intensification occurred slightly earlier than previously suggested based on palynological evidence. The strengthening in the Southern Westerlies during the mid-Holocene is most likely caused by an increase in the temperature gradient as a result of enhanced influence and/or southward migration of the Southeast Pacific anticyclone and a larger Antarctic sea-ice extent.

© 2005 Elsevier B.V. All rights reserved.

Keywords: closed lake basin; magnetic susceptibility; wind intensity; Southern Westerlies; paleoclimate; Patagonia

* Corresponding author. Present address: Department of Geological Sciences, University of Florida, Gainesville, FL 32611, USA. Tel.: +1 352 392 5873; fax: +1 352 392 9294.

E-mail address: agilli@geology.ufl.edu (A. Gilli).

1. Introduction

Few modern regional climates on the globe are as dominated by the persistence and strength of westerly winds, as the climate of Patagonia at the southernmost tip of South America (Prohaska, 1976; Weischet, 1985). This dominance by a single meteorological element is the result of the Southern Westerlies affecting these high southern latitudes. As the Southern Westerlies largely control the precipitation pattern along the southern Andes (Fig. 1B), the past behavior of this westerly storm belt is of special interest. The paucity of multi-proxy paleoclimatic records in this area has led to controversial discussions about the past location of the Southern Westerlies, especially for the time interval of the Last Glacial Maximum (e.g., Heusser, 1989; Markgraf, 1989; Lamy et al., 1999; Jenny et al., 2001). For the early Holocene, there is evidence pointing towards a high southern location of the Southern Westerlies between 45°S and 50°S. The onset of the modern behavior with a seasonal latitudinal shift occurred sometime during the middle Holocene (Markgraf et al., 1992). Since that time, the westerlies storm tracks have migrated equatorward to a latitude of ca. 40°S during austral winter (July), and poleward during austral summer (December), centered around 45°S (Markgraf, 1993, 1998)(Fig. 1B).

Our study site, Lago Cardiel (49°S/71°E, 276 m.a.s.l.) is strongly affected by the Southern Westerlies and, thus, is an ideal location to trace the past behavior of storm tracks. The lake lies on the Patagonian Plateau between the Andean cordillera and the Atlantic coast (Fig. 1A), and it is a hydrologically closed basin with a diameter of approximately 20 km and a modern maximum water depth of 76 m (Fig. 1C). Río Cardiel is the principal, perennial inflowing river draining large parts of the catchment area west of the lake, which consists of deformed Cretaceous/Tertiary shales and flat-lying Tertiary volcanics (Feruglio, 1950; Heinsheimer, 1959; Ramos, 1982). The morphology of the lake basin and the modern climate conditions of the study region are described elsewhere (Gilli et al., 2005). In the past, Lago Cardiel has experienced major lake level changes as documented by previously published research dating fossil shorelines. Galloway et al. (1988) and, in greater detail, Stine and Stine (1990) documented periods of higher than modern lake levels using radiocarbon dating of

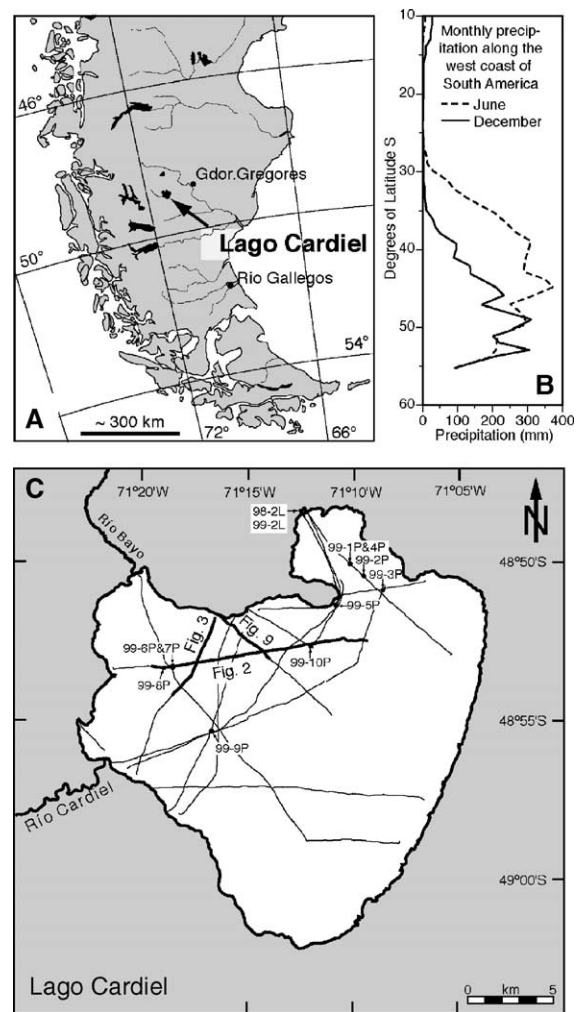


Fig. 1. (A) Map of the southernmost tip of South America showing the location of Lago Cardiel. (B) Monthly precipitation for December and June along the west coast of South America (Lawford, 1996). (C) Map of Lago Cardiel showing the seismic network, the coring sites of all long sedimentary cores and locations of the seismic lines shown in (Figs. 2, 3 and 9).

bulk carbonate deposits from shorelines exposed mainly in stream cuts. Stine and Stine (1990) proposed a major lake level highstand of +55 m around 9500 ^{14}C yr BP, an intermediate highstand around 5000 ^{14}C yr BP and four minor highstands in the last 2000 yr. The sedimentological and paleoecological analysis of on-shore Livingstone piston cores confirmed this early Holocene highstand, as well as variable lake levels during the late Holocene (Markgraf et al., 2003). A study combining high-resolution

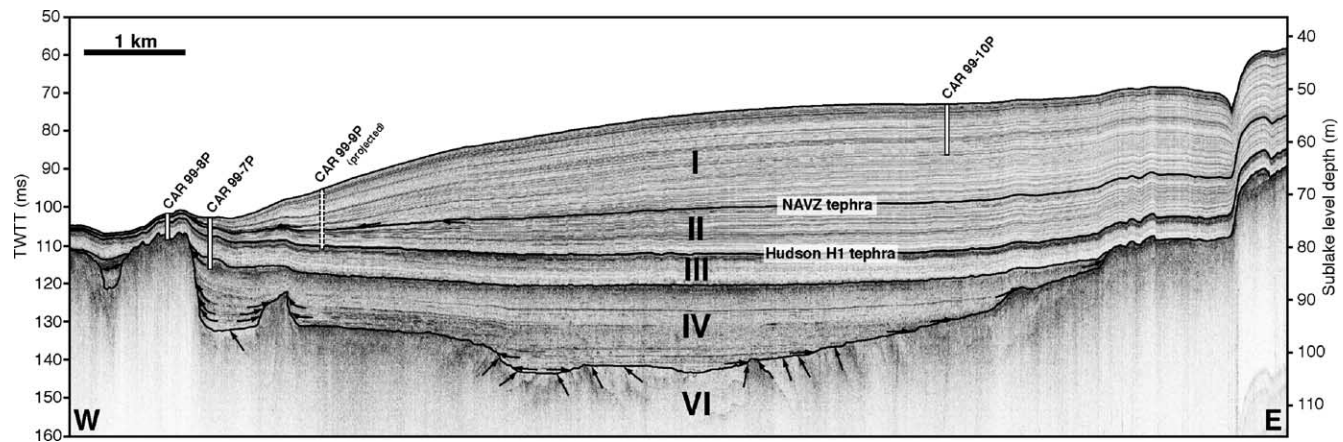


Fig. 2. Interpreted summary seismic profile (W–E) showing the extent of seismic sequences as indicated by roman numerals. Small arrows indicate reflection terminations. The locations of the three cores analyzed in this study CAR 99-7P/9P/10P are also shown. Depth is given in milliseconds (ms) of the two-way travel time (TWTT) and consequently converted to sub-lake level depth (m) based on a P-wave velocity of 1450 m s^{-1} for water and sediment.

seismic and initial core analysis documented for the first time the full spectrum of late Pleistocene lake level fluctuations in Lago Cardiel (Gilli et al., 2001). The detailed seismic stratigraphic analysis revealed a desiccation horizon underlying sediments deposited during much lower lake levels, which in turn are overlain by a second desiccation horizon dated around 11,220 ^{14}C yr. BP. After that time a large transgression apparently resulted in an over 135 m lake level rise forming the previously dated early Holocene lake level highstand at about +55 m (Stine and Stine, 1990). After this transgression, no seismic evidence points towards a significant lowering of the lake level below present-day levels during the entire Holocene.

As the analysis of the seismic profiles revealed large lateral differences in the sedimentation rate (Gilli et al., 2001, 2005), the seismic stratigraphy was crucial in determining the coring locations covering the widest possible stratigraphic range. In this paper, we present sedimentological analyses of three long piston cores, which bring new insights into the depositional system of Lago Cardiel, and allow us to securely assess past variations in the strength of the westerly winds at this latitude.

2. Coring strategy and methods

A ~245 km long grid of seismic lines was acquired during two seismic field campaigns in October/

November 1999 and March 2002. Detailed analysis of these data separated the sedimentary succession into six major seismic sequences (Gilli et al., 2001, 2005) (Fig. 2). Sequence VI, the oldest sequence, is interpreted as the acoustic basement consisting most likely of Cretaceous claystone (Beres et al., submitted for publication) of which only the topmost centimeters were recovered in core CAR 99-8P (Fig. 2) and CAR 99-4P. Sequence V (not shown in Figs. 2 and 3) was beyond the reach of the ETH-Kullenberg coring system (Kelts et al., 1986) and was interpreted as a former alluvial fan (Gilli et al., 2005). A relative shallow and laterally restricted lake was present during Sequence IV, whereas the base of Sequence III represents the large transgression at the beginning of the Holocene. The youngest two Sequences II and I show a high accumulation of sediments in the central part of the lake, and, therefore, a large variation in thickness, being ~28 m close to the depositional center and only a few meters towards the lake shore (Figs. 2 and 3). Based on the described seismic stratigraphy, 10 piston cores with maximal lengths of 12.3 m were retrieved with the ETH-Kullenberg coring system. Three cores (CAR 99-7P, 99-9P and 99-10P) were analyzed in greater detail covering the youngest three sequences (I–III) and the uppermost part of Sequence IV. Core CAR 99-7P (Fig. 2, total core length: 1111.1 cm) penetrated almost 2.5 m into Sequence IV and recovered a complete Sequence III. Sequence II and I are strongly condensed at this coring site. Core CAR

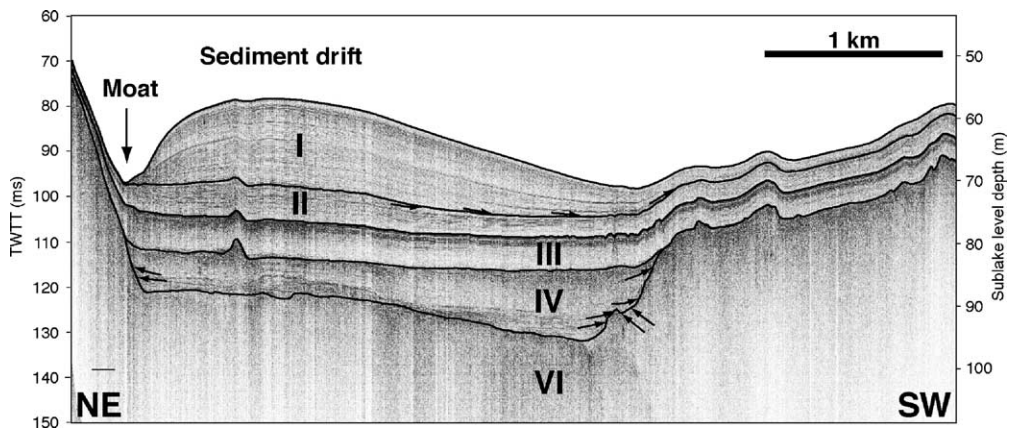


Fig. 3. Seismic reflection profile running perpendicular to the northern border of the Lago Cardiel (see Fig. 1 for exact location). The drift-moat structure is strongly amplified in this part of the lake causing large lateral differences in the thickness of Sequence I and the upper part of Sequence II.

99-9P is located slightly closer to the depositional center and, with a total core length of 1232.7 cm, covers Sequences I, II and part of III. The third core presented here, CAR 99-10P, was recovered near the depositional center on the sediment dome of Sequence I (Fig. 2). With a total length of 1060.1 cm, CAR 99-10P comprises almost two thirds of expanded Sequence I at high resolution. Based on this coring strategy a composite sedimentological record with a length of almost 25 m can be compiled.

The fieldwork involved core retrieval, cutting into 1 m sections, and shipping of the cores to the Limnology Laboratory at the ETH Zürich, Switzerland. They were stored in a dark cold room at 4 °C and scanned prior to opening with a GEOTEK™ multi-sensor core logger to obtain the petrophysical properties (P-wave velocity, gamma-ray attenuation bulk density and magnetic susceptibility) in all cores. After opening, the cores were photographed and described in detail. To examine the total mineralogical content of some selected samples, X-ray diffraction (XRD) was performed on a XDS 200 Scintag™ with continuous measurements between an angle of 5° and 65°. The insolation values were calculated with the Program AnalySeries 1.2 (Paillard et al., 1996) using the solution of Berger (1978).

3. Core chronology and sedimentation rates

The chronology for the three cores is based on tephrochronology and selected AMS radiocarbon dates (Fig. 4 and Table 1). Three tephra layers were sampled from the cores and geochemically fingerprinted by electron microprobe analysis to reference material from the following volcanic eruptions:

- (1) the Reclús volcano at $12,690 \pm 190$ ^{14}C yr BP ($15,330^{+560}_{-1170}$ cal yr BP) (McCulloch and Davies, 2001);
- (2) the Hudson volcano at 6700 ± 65 ^{14}C yr BP (7570^{+110}_{-140} cal yr BP) (Stern, 1991; Naranjo and Stern, 1998);
- (3) one of the three volcanoes in the Northern Austral Volcanic Zone (NAVZ) at 3010 ± 45 ^{14}C yr BP (3230^{+110}_{-170} cal yr BP) (Stern, 1991; Markgraf et al., 2003).

These three tephra layers are excellent chronostratigraphic markers and the prominent appearance of the NAVZ and Hudson H1 tephra in the seismic profiles was used to divide the sedimentary package into the first three sequences (Fig. 2). This tephrochronology was refined by one AMS ^{14}C date on a piece of wood

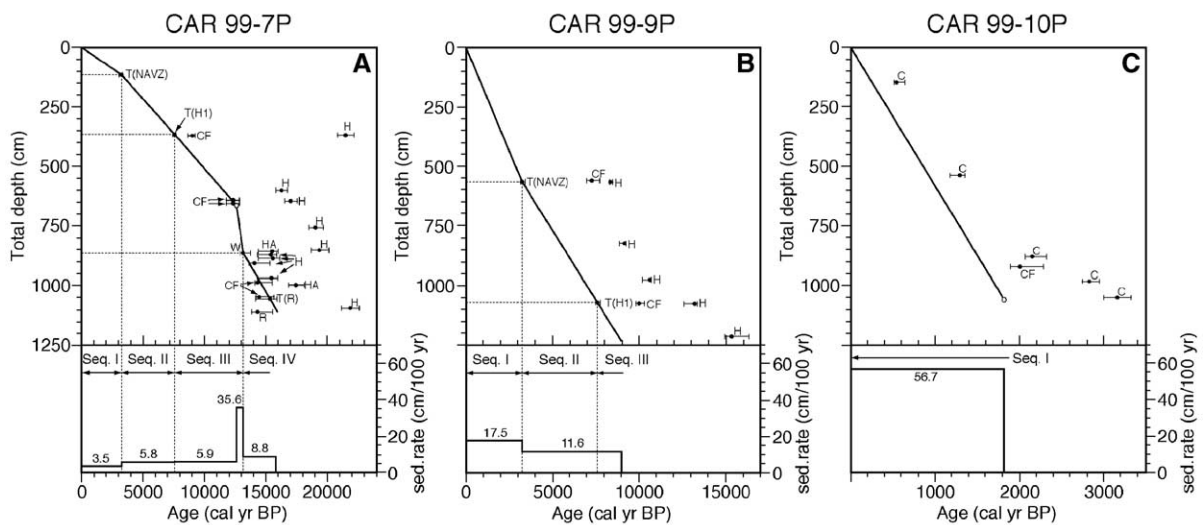


Fig. 4. Age–depth models for the three analyzed cores with the corresponding variation on sedimentation rates (below). Calibrated intercept ages are shown with the 2σ error. Abbreviations for dated materials are: T: Tephra with the name of the eruption in brackets, R: Reclús, H1: Hudson I, NAVZ: Northern Austral Volcanic Zone; W: wood; R: *Ruppia*; H: humin fraction; HA: humic acid fraction; C: bulk carbonate; CF: carbonate fine fraction. Open circles represent estimations in the age model, which are discussed in detail in the text.

Table 1
Radiocarbon dates for the cores CAR 99-7P, CAR 99-9P and CAR 99-10P from Lago Cardiel, Argentina

Core	Section	Sec. depth	Tot. depth	AMS ^{14}C age	$\delta^{13}\text{C}$	Calib. age	Intercept age	Lab. Number	Material/Remarks
		(cm)	(cm)	(yr BP)	(‰)	(cal yr BP)	(cal yr BP)		
CAR 99-7P	0-B	15.5–16.5	114.5	3010 ± 45		3343–3074	3230		NAVZ tephra ^a
CAR 99-7P	4	55–61	366.1	6700 ± 65		7676–7433	7570		Hudson 1 tephra ^b
CAR 99-7P	4	61–62	369.6	18070 ± 65	–27.76	22174–20815	21470	NSRL-13090	Humin fraction
CAR 99-7P	4	62.2–64.0	371.2	8050 ± 65	0.9 ± 1.2	9237–8654	9010	ETH-27330	Carbonate, fine fraction ^c
CAR 99-7P	6	92–93	601.6	13560 ± 65	–24.65	16772–15827	16280	NSRL-13091	Humin fraction
CAR 99-7P	7	33–33.5	641.85	10370 ± 75	3.8	12824–11772	12320	ETH-28325	Carbonate, fine fraction ^c
CAR 99-7P	7	37–38	646.1	14200 ± 55	–25.00 ^d	17539–16548	17020	NSRL-13092	Humin fraction
CAR 99-7P	7	46.5–47	655.35	10370 ± 75	3.2	12824–11772	12320	ETH-28326	Carbonate, fine fraction ^c
CAR 99-7P	7		663.6				12590		Assumption: start of lake level
CAR 99-7P	8	48–49	757.6	15960 ± 55	–25.78	19674–18474	19050	NSRL-13093	Humin fraction
CAR 99-7P	9	43–44	853.1	16240 ± 170	–21.6 ± 1.2	20109–18676	19370	ETH-22767	Humin fraction
CAR 99-7P	9	47.5–48.5	857.6	12860 ± 110	–25.00 ^d	15980–14399	15490	NSRL-12383	Humic acid fraction
CAR 99-7P	9	53–59	865.6	11220 ± 85	–24.3 ± 1.2	13763–12906	13160	ETH-22124	Piece of wood in gravel
CAR 99-7P	9	62–63	872.1	12750 ± 120	–20.8 ± 1.2	15859–14310	15390	ETH-22766	Humin fraction
CAR 99-7P	9	77–78	887.1	12920 ± 170	–22.5 ± 1.2	16136–14379	15550	ETH-22765	Humin fraction
CAR 99-7P	9	97.5–98.5	907.6	11990 ± 110	–21.2 ± 1.2	15322–13636	14060	ETH-22764	Humin fraction
CAR 99-7P	10	58–59	968.6	12790 ± 160	–19 ± 1.2	15965–14302	15430	ETH-22763	Humin fraction
CAR 99-7P	10	76–77	986.6	12390 ± 85	–0.2	15509–14114	14330	ETH-28327	Carbonate, fine fraction ^c
CAR 99-7P	10	87–88	997.6	14570 ± 160	–25.00 ^d	18094–16851	17450	NSRL-12384	Humic acid fraction
CAR 99-7P	11	37.5–38.2	1048.5	12600 ± 85	–1.9 ± 1.2	15636–14203	14450	ETH-27332	Carbonate, fine fraction ^c
CAR 99-7P	11	45–45.5	1055.9	12690 ± 190		15894–14161	15330		Reclus tephra ^c
CAR 99-7P	11	83–84	1094.1	18400 ± 95	–22.34	22594–21168	21850	NSRL-12385	Humin fraction
CAR 99-7P	11	99–100	1110.1	12340 ± 135	–20.6 ± 1.2	15506–13852	14310	ETH-22125	Ruppia and Chara macro rests
CAR 99-9P	6	26–28	560.1	6310 ± 150	3.9 ± 1.2	7553–6802	7250	ETH-27329	Carbonate, fine fraction ^c
CAR 99-9P	6	31.2–32.5	564.9	3010 ± 45		3343–3074	3230		NAVZ tephra ^a
CAR 99-9P	6	32.5–33.5	566.1	7470 ± 35	–25.58	8368–8179	8330	NSRL-13097	Humin fraction
CAR 99-9P	8	88–89	823.7	8190 ± 35	–26.06	9395–9026	9130	NSRL-13098	Humin fraction
CAR 99-9P	10	41–42	975.7	9420 ± 40	–25.53	11036–10508	10610	NSRL-13099	Humin fraction
CAR 99-9P	11	33.8–38.5	1069.85	6700 ± 65		7676–7433	7570		Hudson 1 tephra ^b
CAR 99-9P	11	39–40.5	1073.45	11310 ± 40	–26.76	13774–13028	13180	NSRL-13100	Humin fraction
CAR 99-9P	11	40–41.5	1074.45	8875 ± 70	0.6 ± 1.2	10209–9696	10010	ETH-27328	Carbonate, fine fraction ^c
CAR 99-9P	12	80–81	1213.7	12680 ± 50	–25.65	15703–14303	15320	NSRL-13101	Humin fraction
CAR 99-10P	1	88–89	147	550 ± 35	3.21	643–514	540	NSRL-12386	Bulk carbonate
CAR 99-10P	5	86–87	538.1	1380 ± 50	3.05	1351–1185	1290	NSRL-12387	Bulk carbonate
CAR 99-10P	9	23–24	879.6	2180 ± 35	2.83	2324–2067	2150	NSRL-12388	Bulk carbonate
CAR 99-10P	9	65.5–66.5	922.1	2075 ± 50	–1.4 ± 1.2	2290–1901	2010	ETH-27331	Carbonate, fine fraction ^c
CAR 99-10P	10	24–25	982.1	2730 ± 55	2.55	2950–2750	2830	NSRL-12389	Bulk carbonate
CAR 99-10P	10	92–93	1050.1	2980 ± 35	2.81	3320–3001	3160	NSRL-12390	Bulk carbonate
CAR 99-10P	10		1060.1				1820		Assumption: base of core CAR 99-10P

found in core 7P at the Sequence boundary IV/III revealing an age of $11,220 \pm 85$ ^{14}C yr BP ($13,160^{-250}/_{+600}$ cal yr BP) and four selected AMS ^{14}C dates on the carbonate fine fraction (see footnote c in Table 1 for a detailed description of the preparation of this fraction) taken in the lower part of Sequence III and within Sequence IV. Further 18 AMS ^{14}C datings were conducted on different components of lacustrine organic material (i.e., aquatic plant, humin (acid washed, alkali insoluble) and humic acid (acid washed, alkali soluble) fractions), as well as 9 AMS ^{14}C measurements on carbonates (Table 1). However, a comparison of the ages of these different fractions with the well-dated tephra layers revealed significant offsets of up to several thousand years towards older ages and, therefore, are not included in the chronology of the cores (Fig. 4). All calendar ages were computed using the radiocarbon calibration program CALIB v 4.3 (Stuiver and Reimer, 1993; Stuiver et al., 1998) reporting the 2σ range and the intercept age (Table 1).

3.1. Core CAR 99-7P

The age model of core CAR 99-7P (Fig. 4A) is based on the linear interpolation among the three tephra layers from the eruption of the volcanoes NAVZ, Hudson 1 and Reclús, one ^{14}C date obtained on a ~5 cm large piece of wood at the Sequence boundary VI/III and two ^{14}C dates on the carbonate fine fraction determining the onset of the lake level rise in the lower part of Sequence III. Two further ^{14}C dates on the carbonate fine fraction within Sequence IV confirm the proposed chronology.

The sedimentation rate for core 7P varies considerably between 3.5 and 35.6 cm/100 yr (see Fig. 4A). The highest sedimentation rate occurred at the beginning of Sequence III with the deposition of silty dry

clay (see discussion later) and subsequently decreases towards the core top; Sequences II and I are condensed (Figs. 2 and 3). A slightly higher sedimentation rate of 8.8 cm/100 yr is indicated for the cored section of Sequence IV.

3.2. Core CAR 99-9P

The chronology of core CAR 99-9P was established by linear interpolation between the Hudson H1 and NAVZ tephra layers (Fig. 4B). This indicates a sedimentation rate for Sequence III and II of 11.6 cm/100 yr and for Sequence I of 17.5 cm/100 yr.

3.3. Core CAR 99-10P

The 10.6 m long core 10P was recovered from the depositional center of Sequence I, where this sequence has a total thickness of over 18 m (Fig. 2). Therefore, no tephra layer is found in the retrieved core and its chronology is established based on a linear interpolation within Sequence I derived from the seismic data. An age of 1820 cal yr BP is then attributed to the base of core 10P implying a very high sedimentation rate of 56.7 cm/100 yr (Fig. 4C) for this interval.

3.4. Causes for the discrepancy in radiocarbon ages

With a few exceptions within Sequence IV and III, all radiocarbon ages reveal an offset of at least several hundred years to the age models mainly based on the well-dated tephra layers. This raises questions about (1) the cause of the age offsets and (2) the variation in the offsets among the different fractions.

- (1) The documented age offset between the radiocarbon dates of different fractions and the proposed chronology is most likely the result of a

Notes to Table 1:

All ages were calibrated using CALIB 4.3 (Stuiver and Reimer, 1993). In case of several intercept ages, the one closest to the highest probability was chosen and rounded to the nearest ten.

^a Markgraf et al. (2003).

^b Naranjo and Stern (1998); the age was calibrated with an estimated radiocarbon error of ± 65 yr.

^c For the carbonate fine fraction, the samples were wet sieved through an 11 μm textile mesh using distilled water buffered with NH_4 (resulting pH=7.5–8). A very tiny amount of Triton®X-100 detergent was added to increase the dispersion of the particles. The resulting suspension was centrifuged, freeze-dried, and subsequently submitted for AMS ^{14}C dating.

^d Estimated.

^e McCulloch and Davies (2001).

variable radiocarbon reservoir effect. Weathering of old carbonate sediments releases ^{14}C free carbon into the basin changing the initial $^{14}\text{C}/^{12}\text{C}$ ratio of the lake water (Broecker and Walton, 1959). In a lacustrine system with rapidly changing lake levels, such as documented for Lago Cardiel, dating problems related to differential weathering were expected. A second process controlling this initial carbon ratio is the exchange rate of carbon with the atmospheric reservoir. Geyh et al. (1998) proposed that the radiocarbon reservoir effect is dependent on the water depth as this effect is, among others, a function of the volume/surface ratio of the lake. The only fraction clearly showing this relationship is the carbonate fine fraction with almost no reservoir effect during the lake level lowstand of Sequence IV and at the beginning of the lake level rise in Sequence III. In contrast, carbonate fine fraction dates on sediments deposited in times of intermediate lake level reveal significant offsets from the known ages of the tephra layers (see Fig. 4A and B). Dates from other fractions are either restricted to some core sections, or they show a certain consistency in their offset independent of the lake level evolution (i.e., the humin dates over the transgression at the beginning of Sequence III; Fig. 4A). Furthermore, a contamination due to the erosion of older sediment material deposited during lake level highstands might be an important factor.

- (2) Discrepancies in the age of different fractions have been documented earlier by several authors (Fowler et al., 1986; Geyh et al., 1998; Walker and Harkness, 1990; Lowe and Walker, 2000; Xu and Zheng, 2003) and cannot be explained solely by the presence of the reservoir effect. There is a lack of consensus in the literature about the reliability of the ^{14}C ages of different organic fractions. Some studies (Walker and Harkness, 1990; Walker et al., 2001; Xu and Zheng, 2003) point towards a general younger age of the humic acid fraction than of the humin components, which is likely more affected by the incorporation of old carbon and is, therefore, assumed to be less reliable in specific environments. On the other

hand, humic acids are mobile in most sediments and are, thus, more susceptible to contamination. However, the two humic acid dates in core 7P show a relatively small offset when compared to the majority of the humin fraction dates. Nevertheless, further systematic investigations are needed to understand the response of the different dated fractions to lake level changes.

4. Petrophysical and sedimentological results

All cores were divided into lithological units, which are neither necessarily coinciding to the seismic stratigraphic sequences IV–I, nor can they be correlated among the cores. Seismic sequences have been assigned to the retrieved cores by using a P-wave velocity of 1450 m/s. This is in good agreement with the measured velocity on the sedimentary cores by multi-sensor core logger. In general, all three cores revealed persistent high amounts of quartz and clay minerals, especially smectite and in much lower concentrations kaolinite. This mineralogical composition clearly points towards dominantly detrital sedimentation in the Cardiel basin.

4.1. Core CAR 99-7P

Six lithological units can be identified in core CAR 99-7P covering seismic sequences IV to I (Fig. 5). The oldest sediments of lithological unit 6 and 5 coincide with Sequence IV. Lithological unit 6 consists of pale-olive silty clay with 0.5–1.0 cm thick laminations of slightly finer and lighter-colored layers intercalated with slightly coarse and darker layers. Several white layers, mostly composed of fine-grained authigenic carbonate minerals, can also be identified. The lowest 15 cm of this core contains a high abundance of plant remains, tentatively identified as *Ruppia* sp. The 0.5 cm thick Reclús tephra layer at 1055.9 cm shows only a small peak in density and magnetic susceptibility. A dark grayish to blackish color of speckled and sometimes lenticular appearance was found in the lower part of lithological unit 5, which faded away immediately after core opening. This dark color originates most likely from the presence of iron monosulfides. The upper

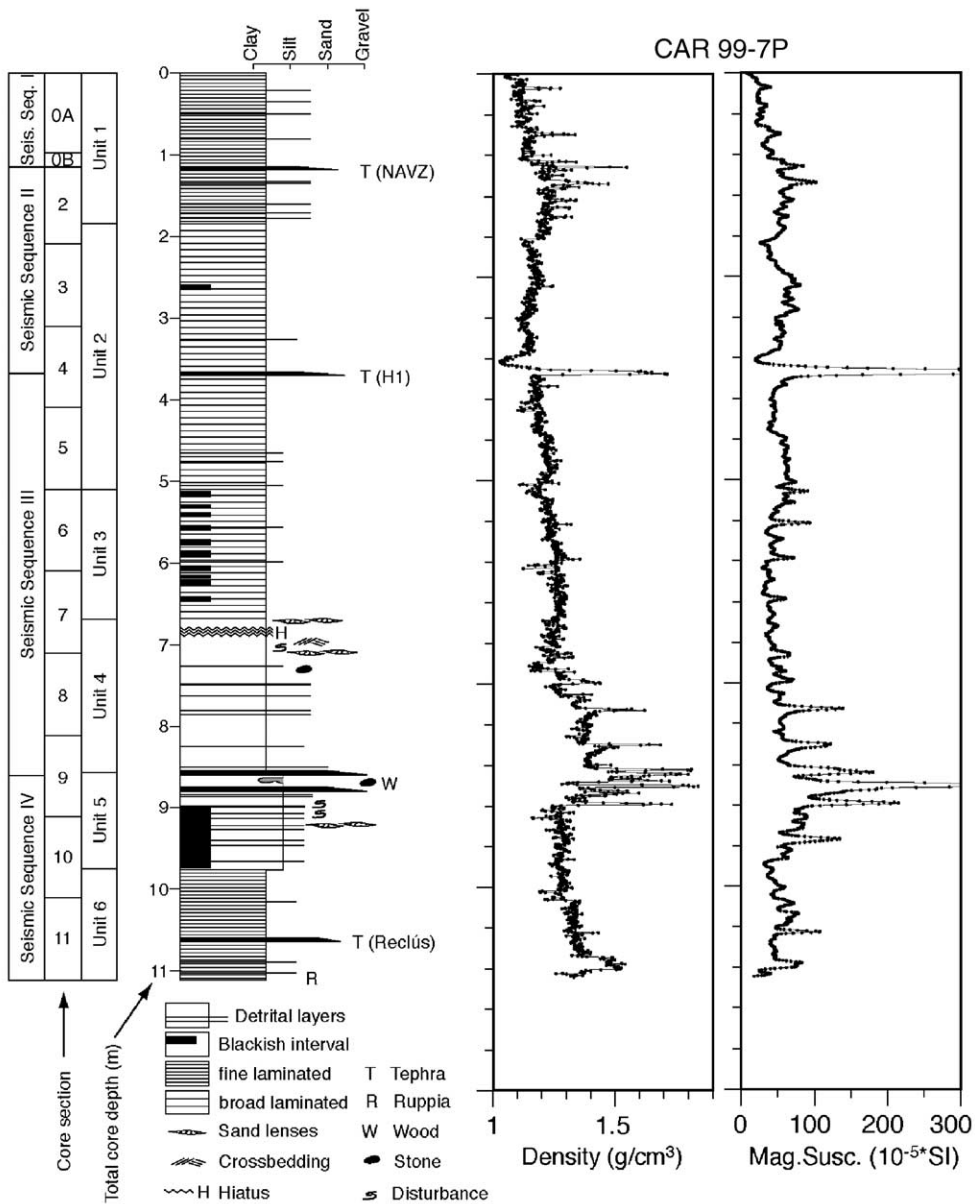


Fig. 5. Lithological column of core CAR 99-7P with the petrophysical data of density and magnetic susceptibility.

part of lithological unit 5 consists of light-olive to yellowish-gray coarse silty clay with several distinct graded sand layers. This is also reflected by the general increase and strong variability of density, as well as magnetic susceptibility. Some of the sand layers are lenticular in shape, and disturbed bedding is present in this part of the core. At a depth of

862.6–868.6 cm, a large piece of wood was present within a sandy and gravelly peat matrix. Above this layer, an almost 2 m-thick sedimentary package is found with sticky silty clay and some sandy layers, which characterize lithological unit 4. A ~1 cm-diameter pebble, sand lenses and well-developed cross ripples are found in the upper part of this lithological

unit. At the top of lithological unit 4, three distinct hiatuses occur within folded and disturbed sediments and are overlain by a 7 cm-thick interval of lenticular sand layers. A sharp change in lithology occurs at the base of lithological unit 3, which consists of fine-laminated silty clay with abundant light colored car-

bonate layers. The thickness of the laminations varies between 0.2 and 0.5 cm, but increases towards the top of this lithological unit. Ten blackish intervals with a thickness of approximately 1 to 5 cm appear at an almost constant interval of 15 to 20 cm. The youngest lithological unit 1 consists of laminated

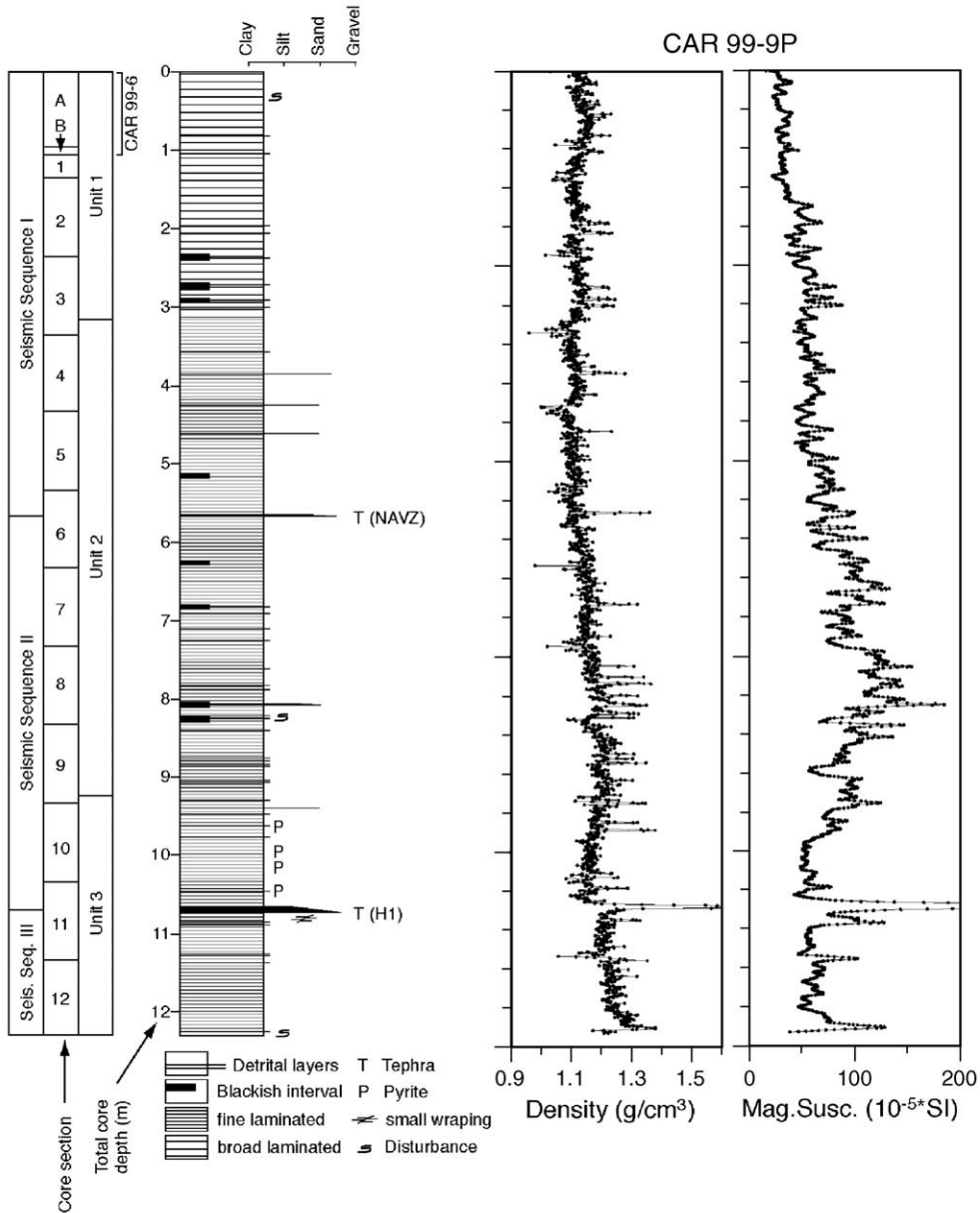


Fig. 6. Lithological column of core CAR 99-9P with the petrophysical data of density and magnetic susceptibility.

silty clay with some broad light-colored carbonate layers. The thickness of the lamination ranges between 0.5 and 1.0 cm. The color changes abruptly at the beginning of this lithological unit from light olive gray to a yellowish brown. The NAVZ tephra

layer is present at a total core depth of 114.0–115.0 cm and displays a dominant peak in density. In contrast to the H1 Hudson tephra at around 366.1 cm, it shows only a slight increase in magnetic susceptibility.

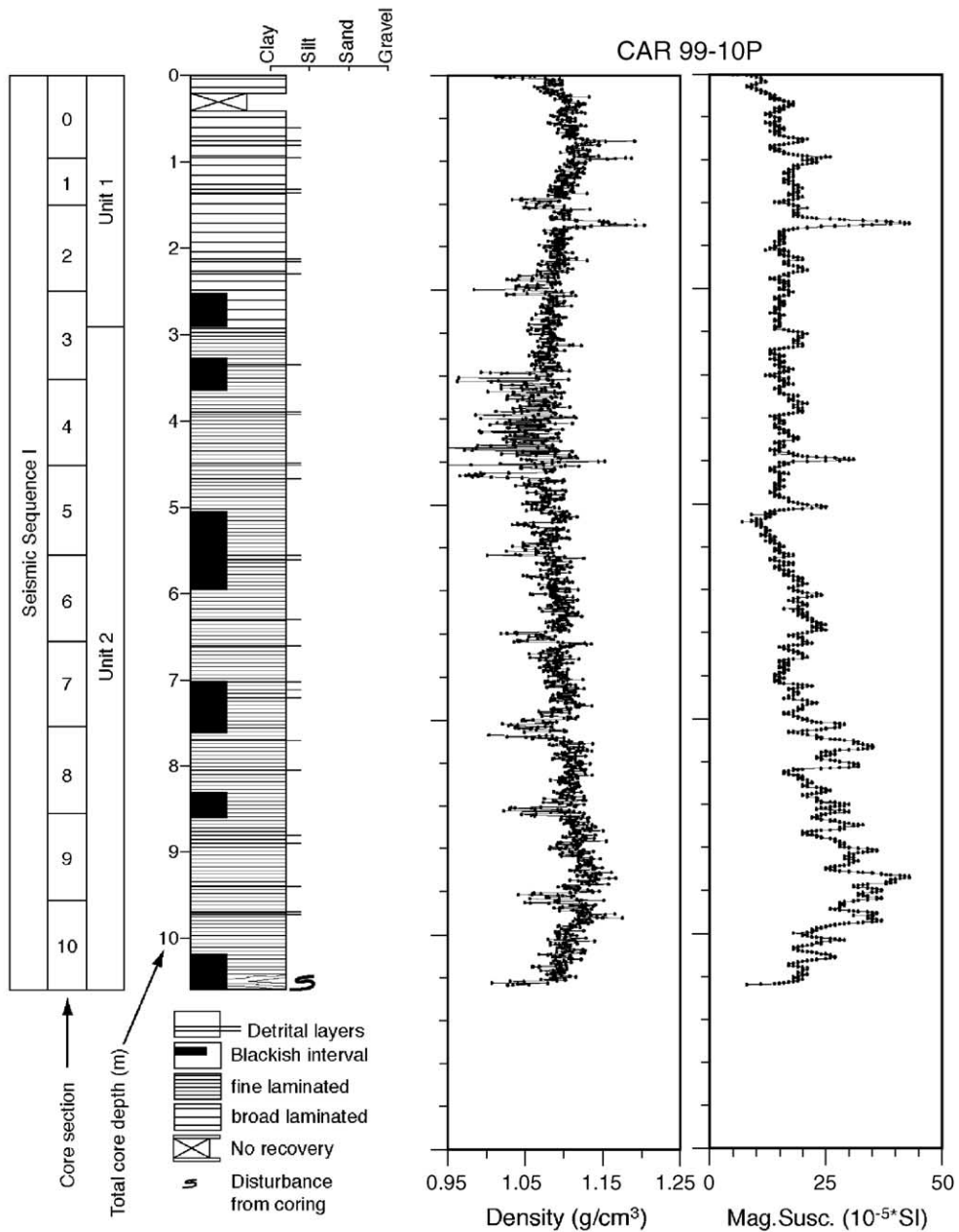


Fig. 7. Lithological column of core CAR 99-10P with the petrophysical data of density and magnetic susceptibility.

4.2. Core CAR 99-9P

Three lithological units can be distinguished in core CAR 99-9P (Fig. 6). The lowest lithological unit 3 consists of light olive gray-colored silty clay with 0.3 to 1.0 cm-thick laminations. Embedded within this lithological unit at a depth of 1067.7–1072.3 cm is the Hudson H1 tephra layer with the same characteristics as in core 7P. Just below, small-scale deformation occurs, which is probably the result of the sudden overload of the several centimeter-thick tephra layer. The XRD-analysis of some hand picked grains revealed the presence of pyrite in the upper part of lithological unit 3. SEM analysis confirmed a framboidal morphology of the pyrite grains. The limit between lithological units 2 and 3 is transitional, changing from a light olive gray to a moderate to dark yellowish brown color. The character of the lamination remains similar, but blackish colored layers occur within lithological unit 2. With an identical appearance as in core 7P, the NAVZ tephra layer is found at a depth of 564.3–565.6 cm. The magnetic susceptibility profile shows a well-defined upward increasing trend in the lower part of lithological unit 2 reaching maximum values at a depth of ~750–850 cm, from where it gradually declines to pre-unit 2 values. With the beginning of lithological unit 1 the average thickness of the lamination increases from about 0.3–1.0 to 0.5–2.0 cm. The upper part of lithological unit 1 reveals remarkable constant values for the magnetic susceptibility. A small-scale discordance in a depth of around 62 cm is likely attributed to core disturbance.

4.3. Core CAR 99-10P

Core CAR 99-10P was taken near the depositional center of Sequence I revealing two major lithological units (Fig. 7). Lithological unit 2 consists of light olive gray silty clay with 0.5–1.5 cm-thick laminations. Several intervals of this lithological unit have laminae with a blackish color. The petrophysical analysis of this lithological unit revealed generally elevated values for magnetic susceptibility in the lowest ~130 cm with a subsequent gradual upward decrease to a core depth of ~500 cm. Lithological unit 1 is composed of dark yellowish brown silty clay with a broader lamination between 1 and 2.5 cm. No major

petrophysical trends are recognizable within lithological unit 1.

5. Discussion

5.1. Indication for currents in Lago Cardiel

The analysis of the seismic profiles revealed no indication of any current activity during the deposition of Sequences IV and III. According to the geometry of the reflection onlaps during Sequence IV the lake level was relatively low during this time (Gilli et al., 2005). This low lake level is further confirmed by the occurrence of *Ruppia* at the base of core 7P, which is restricted to a water depth of less than 10 m in Lago Cardiel (Lucchini, 1975). The well-preserved lamination as well as the blackish colored interval in unit 5 of core 7P, most likely points towards reducing bottom water conditions. During the identified lake level lowering leading to a short desiccation at the Sequence boundary IV/III, the sediment became coarser with increased values in density and magnetic susceptibility. In addition, the higher frequency of distinct coarse layers and the occurrence of sand lenses, crossbedding, pebbles, and some gaps point towards a depositional environment proximal to the shore. According to the proposed age model for core 7P, the corresponding sedimentation rate of the sticky clay within lithological unit 4 was rather high during the low lake level at the beginning of Sequence III (Fig. 4). The end of lithological unit 4 is marked by sand lenses and well-developed cross ripples, further supporting a shore-proximal environment. The undisturbed and finely laminated sediments of lithological unit 3 indicate deepening of the lake and, hence, represent the onset of the transgression previously identified in Sequence III. The nearly regular thickness of Sequence III throughout the basin (Fig. 2) is probably the result of an almost homogenous spread of the incoming detrital material by density-driven over- or interflows.

Sequence II and I can be compared in all three cores. A compilation of the three magnetic susceptibility records reveals significant differences (Fig. 8), whereas the density in the three cores does not show any relevant changes. Core 9P shows a significant upward increase in magnetic susceptibility in the

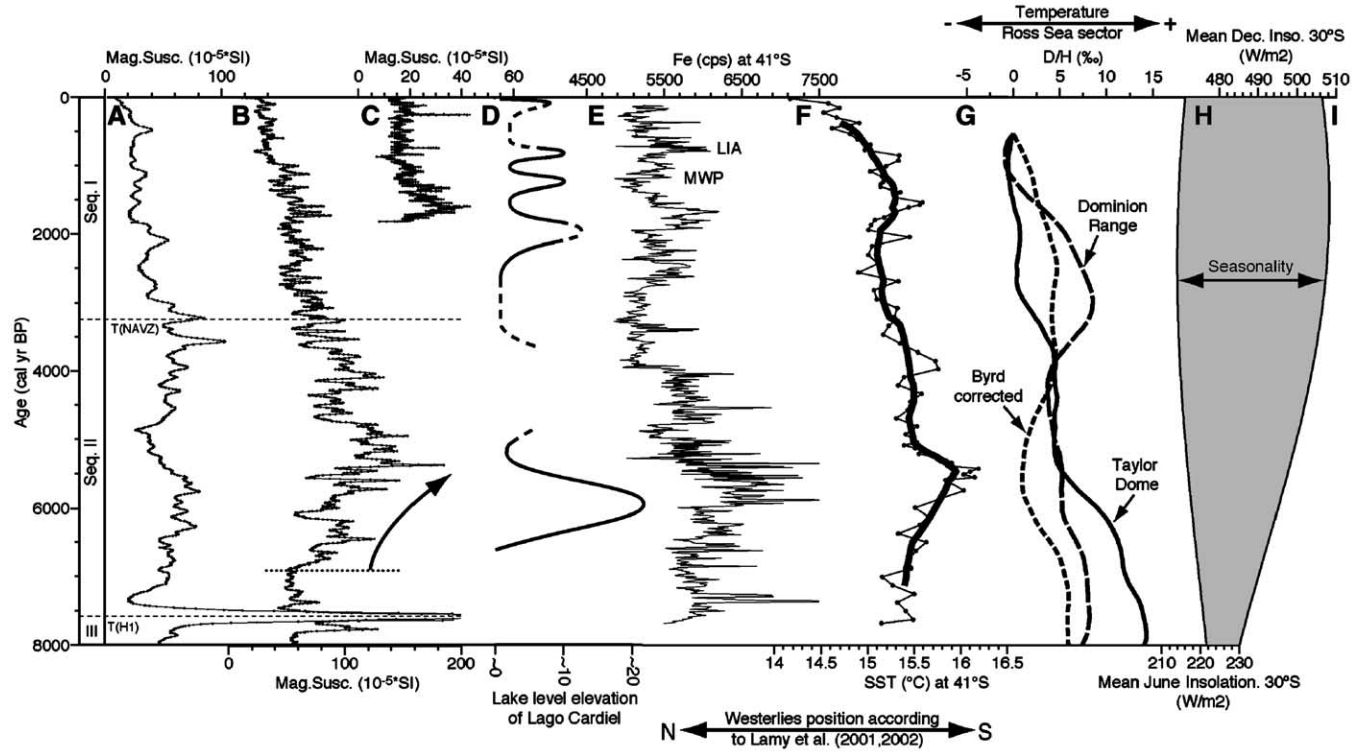


Fig. 8. Comparison among the magnetic susceptibility records of (A) CAR 99-7P; (B) CAR 99-9P; (C) CAR 99-10P; (D) the lake level elevation based on shoreline dating (Stine and Stine, 1990); (E) the iron content in a marine sedimentary core at the Chilean coast at 41°S (Lamy et al., 2001); (F) the sea-surface temperature (SST) at 41°S (Lamy et al., 2002); thick line is an 11-point moving average; (G) centered deuterium trends for three Antarctic ice cores from the Ross Sea sector (Masson et al., 2000) and the mean monthly insolation at 30°S in (H) June and (I) December (Berger, 1978). The difference between the insolation values defines seasonality, which increases during the Holocene. The occurrence of tephra layers, the extent of the seismic sequences and the increase in magnetic susceptibility (arrow) are also indicated.

lower part of Sequence II (arrow in Fig. 8B) with a subsequent decrease towards the top of the core. This trend towards higher magnetic susceptibility values in core 9P coincides with a change in sedimentation expressed as a gradual color change, as well as the disappearance of pyrite between lithological unit 3 and 2 (Fig. 6).

This lithological transition in core 9P coincides with the beginning of the sediment focusing at the onset of drift deposition, as seen in the seismic profiles. The increasing trend in the magnetic susceptibility is most likely caused by an enhanced deposition of magnetic grains at the beginning of the drift formation at this particular core site. In addition, the frequency of distinct coarse layers is enhanced during this time interval, as documented by the increasing occurrence

of peaks in the density record (Fig. 6). A modern analog for the dependency of the magnetic susceptibility on current velocity can be found at the northern border of the lake, where a pronounced moat is present (Figs. 3 and 9). A significant increase in density and magnetic susceptibility as a result of increasing current velocity is documented by a transect of short sediment cores from the depositional center (coring site A) towards the moat (coring site D) (Fig. 9). The interpretation of the subsequent decrease in magnetic susceptibility in core 9P as a decrease in drift activity would conflict with the seismic sequence analysis, which indicates an even stronger sediment focusing during the deposition of Sequence I (Gilli et al., 2005). Therefore, the decrease in magnetic susceptibility is related to the lateral migration of the drift system,

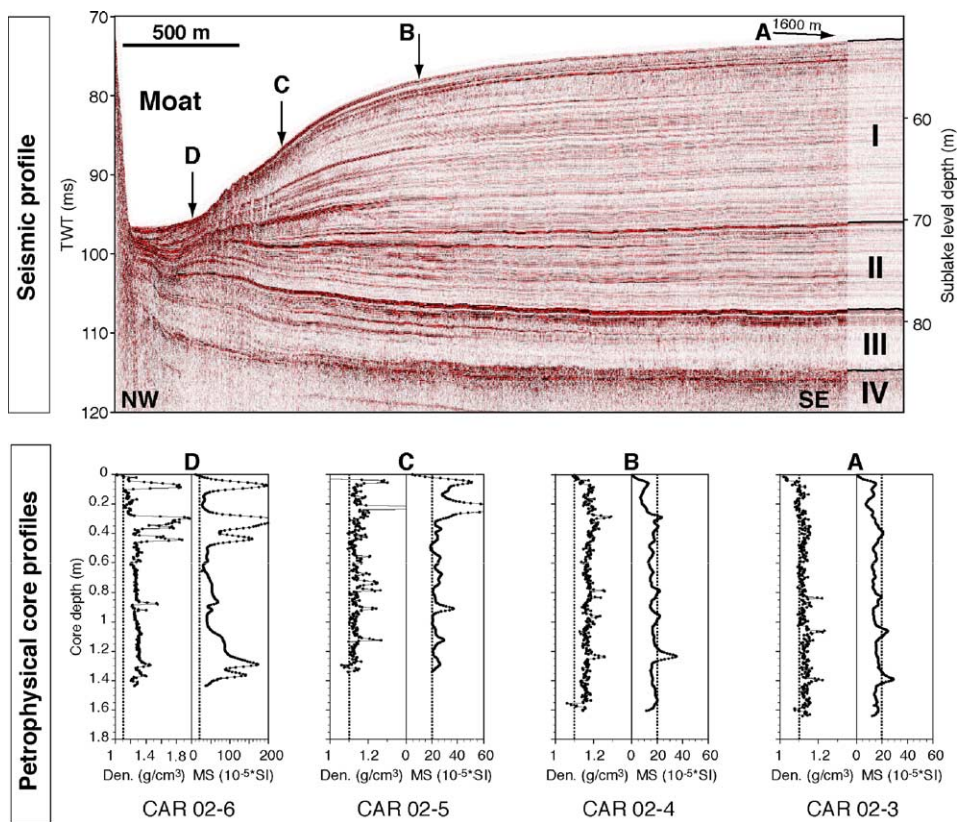


Fig. 9. Seismic profile perpendicular to the moat axis at the northern shore of Lago Cardiel (above) and the density/magnetic susceptibility (MS) results of four short sediment cores taken along this seismic profile (below). An increase in the petrophysical values from Site A to D can be explained by an increase in current velocity towards the moat. Dashed line represents a fixed value, which can be used to visualize the increase in density and magnetic susceptibility; note the changed axis for the petrophysical properties at the Site D. This figure is adopted from Gilli et al. (2005).

which is especially pronounced at the western side of the depositional center (e.g., drift migration towards SW in Fig. 3). The onset of a lake current coincides with the disappearance of pyrite between lithological units 3 and 2 (Fig. 6). The exact reason for this disappearance is difficult to assess as the knowledge about the iron cycle of this lake is limited, but it may be related to an increased availability of oxygen associated with the presence of the lake current and/or an increased freshwater input at this time (Fig. 8D). Both processes are inhibiting the formation of pyrite (Berner, 1970, 1984). The onset of the drift deposition started around ~6800 cal yr BP, as recorded by the changes in the sedimentology and magnetic susceptibility in core 9P (Fig. 8B).

5.2. Implications for wind history

Lake current activity in Lago Cardiel and, thus, drift deposition was most likely triggered by the intensification of the westerly winds affecting this region. The present-day latitudinal distribution of major vegetation types has been interpreted to reflect the seasonal behavior of the southern westerly storm tracks. This is especially the case for the occurrence of the Magellanic Moorland vegetation, which expands only under extremely stormy and high precipitation conditions (Villagran, 1988; Markgraf, 1993, 1998). Pollen analysis in the southern part of South America revealed the onset of the Southern Westerlies' precipitation regime at high southern latitudes in the early Holocene (Markgraf, 1993, 1998). Our record of magnetic susceptibility and the presence of the drift deposition now further documents an intensification of the westerly storm tracks at a latitude of 49°S after 6800 cal yr BP. As the Southern Westerlies is the dominant weather system affecting Lago Cardiel, a lake level highstand at the same time (Stine and Stine, 1990; Fig. 8D) further documents a strengthening of westerly winds. And a third evidence for increased wind activity comes from a change in pollen proportions documented in the shoreline cores of Lago Cardiel by higher percentages of long-distance transported pollen grains from the Andean forests (Markgraf et al., 2003).

A high-resolution paleoceanographic record from core GeoB 3313-1 taken on the Chilean continental slope at 41°S (Lamy et al., 2001, 2002) supports our

interpretation of the past behavior of the Southern Westerlies. Analysis of iron content in the sediment was interpreted to reflect the rainfall distribution in the catchment area. Relative low iron content would relate to enhanced runoff from the iron-poor Coastal Ranges during times when the southern westerly storm tracks were positioned over the latitude of the catchment area. Without the influence of the Southern Westerlies, the sediment material would have mainly been derived from the higher-elevated and iron-rich Andean region causing a relative higher iron influx to the coastal area. Therefore, Lamy et al. (2001) proposed for the Fe-enriched periods between 7700 and 4000 cal yr BP (peaking between 6000 and 5300 cal yr BP) a more poleward position of the Southern Westerlies and, thus, less humid conditions at 41°S (Fig. 8E). After 4000 cal yr BP when Fe was present only in low proportions, the Southern Westerlies would have reached the latitude of 41°S, even though some century-scale peaks in the iron content point towards some short-lived reduced influence of the southern westerly storm tracks. This southward migration of the Southern Westerlies is supported by a synchronous southward shift of the Antarctic Circumpolar Current (ACC). Lamy et al. (2002) related a warming trend in the sea-surface temperature (SST) between 7800 and 5500 yr BP (Fig. 8F) to a decrease in advection of ACC-derived water masses by a southward migration of the ACC. As the position of the ACC and the Southern Westerlies are linked by the steepest temperature gradient, both proxies show a coherent southward migration of the westerly wind belt system (Lamy et al., 2002). In contrast to this marine study, a high-resolution pollen study from the same latitude (41°S) documented a cool and wet climate interval between 7600 and 4100 cal yr BP (Moreno, 2004). This would imply an equatorward shift of the Southern Westerlies, which would be in opposition to the interpretation of Lamy et al. (2001, 2002) and demonstrates the need for further high-resolution paleoclimate records from this area. However, the magnetic susceptibility records from Lago Cardiel reveal some striking similarities with the marine iron record (Fig. 8). The major increase in magnetic susceptibility in core 9P between ~6800 and ~5300 cal yr BP, interpreted as a strengthening of the westerly winds at 49°S, coincides well with a focusing of the westerlies at their more poleward location (Lamy et al., 2001, 2002). This intensification of the Southern Westerlies could also

be responsible for a glacial advance at Fachinal, Chile (46°S) around 6200 cal yr BP (Douglass et al., 2005). The late Holocene magnetic susceptibility record of core 9P is dominated by a gradual decrease in sediment thickness due to the lateral migration of the drift system and does not indicate changes in the generally high accumulation rate. In core 10P, the magnetic susceptibility reveals higher values between ~1800 and 1200 cal yr BP (Fig. 8), which coincides with a period of high iron deposition in the record of Lamy et al., 2001. As the core 10P was recovered close to the depositional center, a change in the magnetic susceptibility is more likely related to a change in the current velocity than due to the migration of the drift deposition. Therefore, this increase in magnetic susceptibility and iron content could indicate a focusing of the wind activity at higher southern latitudes. However, this is not supported by the lake level record showing no related lake level highstand during this time interval (Fig. 8D). Furthermore, the contrasting climate conditions during the Medieval Warm Period (MWP) and the Little Ice Age (LIA) are not recorded in the magnetic susceptibility record of Lago Cardiel as it is in the case of the marine iron record off Chile (Lamy et al., 2001).

5.3. Paleoclimate implications

The documented evolution in the behavior of the Southern Westerlies has major implications for the climate system of the Southern Hemisphere. The general position of the Southern Westerlies is primarily dependent on the location and strength of the Southeast Pacific anticyclone in the north and the circum-Antarctic low pressure belt in the south (Pittock, 1978, p. 225; Aceituno et al., 1993; Markgraf, 1998). The strength of the Southern Westerlies most likely increases with a steeper temperature gradient (Markgraf et al., 1992). At the northern border of the southern westerly wind belt system, the Southeast Pacific anticyclone relates to the migration of the storm tracks. The focusing of the Southern Westerlies after 6800 cal yr BP at higher southern latitudes is probably the result of an intensification and/or southward migration of the Southeast Pacific anticyclone, which deflects the westerly wind belt further south. As a consequence, central Chile received less precipitation as indicated by the iron record at 41°S (Lamy et al., 2001). Several other paleoclimatic records from

central Chile point also towards mid-Holocene aridity (e.g., Villagran and Varela, 1990; Veit, 1996; Lamy et al., 1999; Grosjean, 2001; Jenny et al., 2002) supporting the blocking by the strong Southeast Pacific anticyclone during this time period. This atmospheric situation in the east Pacific resembles the modern La Niña phase (Markgraf et al., 1992), whose dominance in the early and middle Holocene is supported by paleoclimate reconstructions (e.g., Rodbell et al., 1999; Moy et al., 2002) and model simulations (Clement et al., 2000). On the southern boundary of the Southern Westerlies, a cooling and an enlarged extent of sea ice around Antarctica occurred in the middle Holocene. Although the climate evolution in the southern Pacific Ocean is rather poorly documented, there is evidence for a mid-Holocene cooling in this sector of the Southern Ocean and Antarctica. A compilation of ice core records from the Ross Sea sector shows a general decreasing temperature trend after ~7000 cal yr BP (Fig. 8G)(Masson et al., 2000). This is further supported by the methanesulfonic acid concentration in the ice record of Taylor Dome reflecting an increase in sea-ice cover after 6000 cal yr BP (Steig et al., 1998). A similar trend is observed in the East Atlantic Southern Ocean with a general cooling in the summer sea-surface temperature and an increase in the sea-ice presence after 6500 cal yr BP (Nielson et al., 2004), as well as by the occurrence of ice-rafted debris after 5000 cal yr BP (Hodell et al., 2001). These results support a steeper temperature gradient at the southern tip of South America and, thus, to an intensification of the Southern Westerlies as interpreted from the magnetic susceptibility record of Lago Cardiel. This strengthening of the Southern Westerlies is somewhat earlier than previously documented in pollen records from South America, as well as from Australia and New Zealand (Shulmeister, 1999), but can possibly be explained by a direct response of the lake drift system to the wind activity.

Additional constraints for a poleward position of the Southern Westerlies during the early and middle Holocene comes from the insolation characteristics at that time (Markgraf et al., 1992; Markgraf, 1998). Taking into account the orbital parameters defining Earth's insolation, the seasonality contrast in the Southern Hemisphere increased since the beginning of the Holocene (Fig. 8H and I; for further detail see Fig. 3 in Martin et al., 1997). As the earth–sun dis-

tance was minimal in June and maximal in December during the early Holocene, the Southern Hemisphere winters were relatively warmer and the summers cooler than today (i.e., relatively lower seasonality contrast). In the late Holocene, this astronomical configuration reversed and the austral summers were relatively warmer whereas the austral winters turned relatively colder than today. Therefore, the Southern Westerlies were positioned at the modern location during the equinoxes in the late Holocene and started to migrate latitudinal with an increase in seasonality in the middle and late Holocene (Markgraf et al., 1992). This could explain, together with a weakening of the Southeast Pacific anticyclone, the seasonal northward shift of the Southern Westerlies in the middle and late Holocene affecting a latitude of 41°S and even further north. As a consequence of the seasonal migration of the Southern Westerlies, several paleoecological records from southernmost South America revealed an increased variability during the mid- to late Holocene (e.g., Ashworth et al., 1991; Markgraf, 1993; Markgraf et al., 2003). In the late Holocene, core 10P shows an interval of increased magnetic susceptibility between ~1800 and 1200 cal yr BP. This interval coincides with enhanced iron concentration in the coastal marine core at 41°S (Fig. 8E) and is, therefore, probably related to enforced westerly winds in a more southern position.

6. Conclusion

The combined approach using seismic reflection profiling and the analysis of sedimentary cores provides unique tool to disentangle the evolution of closed lake basins (see also: Abbott et al., 2000). With the aid of a well-defined coring strategy combined with a good core-to-core correlation based on seismic investigations and petrophysical data, a composite sedimentary succession with a length of nearly 25 m was established. The chronology of the cores is mainly based on well-dated tephra layers. The near absence of terrestrial organic material and the presence of a radiocarbon reservoir effect limits the establishment of a detailed core chronology, at least for certain time intervals.

Magnetic susceptibility is one of the most sensitive petrophysical sediment parameters in the Lago Cardiel

sedimentary record. Core 9P shows an increase in magnetic susceptibility after ~6800 cal yr BP, indicating the presence of a lake current most likely driven by strong winds. Therefore, this time can be regarded as the beginning of the intensification of the Southern Westerlies at the latitude of 49°S. From a climate system point-of-view, this intensification in the westerly winds of South America can be related to an increase in the temperature gradient driven by the narrowing from the southward migration and/or strengthening of the Southeast Pacific anticyclone and the increased extent of the Antarctic sea ice. The absolute strength of the westerly winds documented by this sedimentary archive is partially masked by the lateral migration of the drift system. Only core 10P, located in the depositional center of the drift, may reveals a higher wind activity between ~1800 and 1200 cal yr BP, which is generally in good agreement with a marine iron record off Chile (Lamy et al., 2001). Our results show the unique possibility to reconstruct past wind conditions in this area of the Southern Hemisphere, which is crucial for paleoclimate modeling. The ongoing analysis of additional geochemical and biological proxies on the sedimentary cores will further refine the reconstruction of the climate conditions in the past with a special focus on the hydrological balance.

Acknowledgements

We would like to thank Jorge Moreteau and his crew for the tireless effort to sail on Lago Cardiel under the above-described harsh and windy conditions. We are grateful to Jean Captain, Antoinette Lüdin, Platt Bradbury and Robert Hofmann for assistance in the field, as well as to, Rossana Martini, Rolf Warthmann and Urs Gerber for help in the lab. We thank Valerie Masson-Delmotte and Frank Lamy for the provided data. Comments by F. Lamy, B.L. Valero-Garces and an anonymous reviewer are acknowledged. This study is part of the PATO/PaLa-Tra project, which is co-founded by the U.S. National Science Foundation grants NSF-EAR-9709145, NSF-ATM-008267 and NSF-ATM-0081279 to V. Markgraf/K. Kelts; and by the Swiss National Science Foundation grants N° 21-50862.97 and N° 20-61704.00/1 to the ETH and University of Geneva

limnogeology groups. The authors thank Blackwell Publishing/International Association of Sedimentologists (IAS) for the permission to reproduce Fig. 9. ^{14}C analyses were partly performed at the AMS Facility, jointly operated by the Swiss Federal Institute of Technology, Zurich and Paul Scherrer Institute, Villigen, Switzerland. Major element analyses of tephra samples were carried out at the Electron Microprobe facility at the School of GeoSciences, The University of Edinburgh, Scotland.

References

- Abbott, M.B., Finney, B.P., Edwards, M.E., Kelts, K.R., 2000. Lake-level reconstructions and paleohydrology of Birch Lake, Central Alaska, based on seismic reflection profiles and core transects. *Quaternary Research* 53 (2), 154–166.
- Aceituno, P., Fuenzalida, H., Rosenblüth, B., 1993. Climate along the extratropical west coast of South America. In: Mooney, H.A., Fuentes, E.R., Kronberg, B.I. (Eds.), *Earth System Responses to Global Change*. Academic Press, San Diego, pp. 61–69.
- Ashworth, A.C., Markgraf, V., Villagran, C., 1991. Late Quaternary climatic history of the Chilean channels based on fossil pollen and beetle analyses, with an analysis of the modern vegetation and pollen rain. *Journal of Quaternary Science* 6 (4), 279–291.
- Beres, M., Gilli, A., Ariztegui, D., Anselmetti, F.S., submitted for publication. History of the Lago Cardiel basin, Argentina (49°S), revealed by multi-channel seismic reflection methods. *Journal of South American Earth Sciences*.
- Berger, A.L., 1978. Long-term variations of daily insolation and Quaternary climatic change. *Journal of the Atmospheric Sciences* 35 (12), 2362–2367.
- Berner, R.A., 1970. Sedimentary pyrite formation. *American Journal of Science* 268 (1), 1–23.
- Berner, R.A., 1984. Sedimentary pyrite formation — an update. *Geochimica Et Cosmochimica Acta* 48 (4), 605–615.
- Broecker, W.S., Walton, A., 1959. The geochemistry of C-14 in fresh-water systems. *Geochimica Et Cosmochimica Acta* 16 (1–3), 15–38.
- Clement, A.C., Seager, R., Cane, M.A., 2000. Suppression of El Niño during the Mid-Holocene by changes in the Earth's orbit. *Paleoceanography* 15 (6), 731–737.
- Douglass, D.C., Singer, B.S., Kaplan, M.R., Ackert, R.P., Mickelson, D.M., Caffee, M.W., 2005. Evidence of Early Holocene glacial advances in southern South America from cosmogenic surface-exposure dating. *Geology* 33 (3), 237–240.
- Feruglio, E., 1950. Descripción Geológica de la Patagonia, III. Dirección Nacional de Yacimientos Fiscales, Buenos Aires. 431 pp.
- Fowler, A.J., Gillespie, R., Hedges, R.E.M., 1986. Radiocarbon dating of sediments. *Radiocarbon* 28 (2A), 441–450.
- Galloway, R.W., Markgraf, V., Bradbury, J.P., 1988. Dating shorelines of lakes in Patagonia, Argentina. *Journal of South American Earth Sciences* 1 (2), 195–198.
- Geyh, M.A., Schotterer, U., Grosjean, M., 1998. Temporal changes of the C-14 reservoir effect in lakes. *Radiocarbon* 40 (2), 921–931.
- Gilli, A., Anselmetti, F.S., Ariztegui, D., Bradbury, J.P., Kelts, K.R., Markgraf, V., McKenzie, J.A., 2001. Tracking abrupt climate change in the Southern Hemisphere: a seismic stratigraphic study of Lago Cardiel, Argentina (49°S). *Terra Nova* 13 (6), 443–448.
- Gilli, A., Anselmetti, F.S., Ariztegui, D., Beres, M., McKenzie, J.A., Markgraf, V., 2005. Seismic stratigraphy, buried beach ridges and contourite drifts: the Late Quaternary history of the closed Lago Cardiel basin, Argentina (49°S). *Sedimentology* 52 (1), 1–23.
- Grosjean, M., 2001. Mid-Holocene climate in the south-central Andes: humid or dry? *Science* 292 (5526), 2391–2392.
- Heinsheimer, J.J., 1959. El Lago Cardiel. *Anales Academia Argentina Geografia* 3, 86–132.
- Heusser, C.J., 1989. Climate and chronology of Antarctica and adjacent South America over the past 30,000 yr. *Palaeogeography, Palaeoclimatology, Palaeoecology* 76 (1–2), 31–37.
- Hodell, D.A., Kanfoush, S.L., Shemesh, A., Crosta, X., Charles, C.D., Guilderson, T.P., 2001. Abrupt cooling of Antarctic surface waters and sea ice expansion in the South Atlantic sector of the Southern Ocean at 5000 cal yr B.P. *Quaternary Research* 56 (2), 191–198.
- Jenny, B., Rondanelli, M., Valero-Garces, B.L., Burns, S.J., Veit, H., Geyh, M., 2001. Moisture changes in central Chile for the last >46,000 years — the Launa de Tagua Tagua record (34°30'S). In: Jenny B. (Ed.), *Climate change in central Chile*, unpublished PhD, University of Bern.
- Jenny, B., Valero-Garces, B.L., Villa-Martinez, R., Urrutia, R., Geyh, M., Veit, H., 2002. Early to Mid-Holocene aridity in central Chile and the Southern Westerlies: the Laguna Aculeo record (34°S). *Quaternary Research* 58 (2), 160–170.
- Kelts, K., Briegel, U., Ghilardi, K., Hsu, K., 1986. The limnogeology-ETH coring system. *Schweizerische Zeitschrift für Hydrologie* 48 (1), 104–115.
- Lamy, F., Hebbeln, D., Wefer, G., 1999. High-resolution marine record of climatic change in mid-latitude Chile during the last 28,000 years based on terrigenous sediment parameters. *Quaternary Research* 51 (1), 83–93.
- Lamy, F., Hebbeln, D., Röhl, U., Wefer, G., 2001. Holocene rainfall variability in southern Chile: a marine record of latitudinal shifts of the Southern Westerlies. *Earth and Planetary Science Letters* 185 (3–4), 369–382.
- Lamy, F., Rühlemann, C., Hebbeln, D., Wefer, G., 2002. High- and low-latitude climate control on the position of the southern Peru–Chile current during the Holocene. *Paleoceanography* 17 (2), 1028. doi: 10.1029/2001PA000727.
- Lawford, R.G., 1996. North–south variations in west coast hydro-meteorological parameters and their significance for earth systems. In: Lawford, R.G., Alaback, P.B., Fuentes, E. (Eds.), *High-Latitude Rainforests and Associated Ecosystems of the West Coast of the Americas*. Springer, New York, pp. 3–26.
- Lowe, J.J., Walker, M.J.C., 2000. Radiocarbon dating the last glacial–interglacial transition (ca. 14–9 C-14 ka BP) in terres-

- trial and marine records: the need for new quality assurance protocols. *Radiocarbon* 42 (1), 53–68.
- Lucchini, L., 1975. Estudio ecológico preliminar de las diatomeas perifíticas y bentónicas como alimento de anfípodos lacustres (Lago Cardiel, Prov. Santa Cruz). *Physis. Sección B. Las Aguas Continentales y Sus Organismos Buenos Aires* 34, 85–97.
- Markgraf, V., 1989. Palaeoclimates in Central and South America since 18,000 BP based on pollen and lake-level records. *Quaternary Science Reviews* 8 (1), 1–24.
- Markgraf, V., 1993. Palaeoenvironments and paleoclimates in Tierra del Fuego and southernmost Patagonia, South America. *Palaeogeography, Palaeoclimatology, Palaeoecology* 102 (1–2), 53–68.
- Markgraf, V., 1998. Past climates of South America. In: Hobbs, J.E., Lindesay, J.A., Bridgman, H.A. (Eds.), *Climates of the Southern Continents: Present, Past and Future*. John Wiley and Sons Ltd., pp. 249–264.
- Markgraf, V., Dodson, J.R., Kershaw, A.P., McGlone, M.S., Nicholls, N., 1992. Evolution of Late Pleistocene and Holocene climates in the circum-South Pacific land areas. *Climate Dynamics* 6, 193–211.
- Markgraf, V., Bradbury, J.P., Schwab, A., Burns, S.J., Stern, C., Ariztegui, D., Gilli, A., Anselmetti, F.S., Stine, S., Maidana, N., 2003. Holocene palaeoclimates of southern Patagonia: limnological and environmental history of Lago Cardiel, Argentina (49°S). *Holocene* 13 (4), 581–591.
- Martin, L., Bertaux, J., Correge, T., Ledru, M.P., Mourguiart, P., Sifeddine, A., Soubies, F., Wirrmann, D., Suguio, K., Turcq, B., 1997. Astronomical forcing of contrasting rainfall changes in tropical South America between 12,400 and 8800 cal yr BP. *Quaternary Research* 47 (1), 117–122.
- Masson, V., Vimeux, F., Jouzel, J., Morgan, V., Delmotte, M., Ciais, P., Hammer, C., Johnsen, S., Lipenkov, V.Y., Mosley-Thompson, E., Petit, J.-R., Steig, E.J., Stievenard, M., Vaikmae, R., 2000. Holocene climate variability in Antarctica based on 11 ice-core isotopic records. *Quaternary Research* 54 (3), 348–358.
- McCulloch, R.D., Davies, S.J., 2001. Late-Glacial and Holocene palaeoenvironmental change in the central Strait of Magellan, southern Patagonia. *Palaeogeography, Palaeoclimatology, Palaeoecology* 173 (3–4), 143–173.
- Moreno, P.I., 2004. Millennial-scale climate variability in northwest Patagonia over the last 15,000 yr. *Journal of Quaternary Science* 19 (1), 35–47.
- Moy, C.M., Seltzer, G.O., Rodbell, D.T., Anderson, D.M., 2002. Variability of El Niño/southern oscillation activity at millennial timescales during the Holocene epoch. *Nature* 420 (6912), 162–165.
- Naranjo, J.A., Stern, C.R., 1998. Holocene explosive activity of Hudson Volcano, southern Andes. *Bulletin of Volcanology* 59 (4), 291–306.
- Nielson, S.H.H., Koç, N., Crosta, X., 2004. Holocene climate in the Atlantic sector of the Southern Ocean: controlled by insolation or oceanic circulation? *Geology* 32 (4), 317–320.
- Paillard, D., Labeyrie, L., Yiou, P., 1996. Macintosh program performs time-series analysis. *Eos, Transactions, American Geophysical Union* 77, 379.
- Pitcock, A.B., 1978. *Climatic Change and Variability — a Southern Perspective*. Cambridge University Press, Cambridge. 455 pp.
- Prohaska, F., 1976. The climate of Argentina, Paraguay and Uruguay. In: Schwerdfeger, W. (Ed.), *Climates of Central and South America*. Elsevier, Amsterdam, pp. 13–112.
- Ramos, V.A., 1982. Geología de la región del Lago Cardiel, Provincia de Santa Cruz. *Asociación Geológica Argentina, Revista* 37 (1), 23–49.
- Rodbell, D.T., Seltzer, G.O., Anderson, D.M., Abbott, M.B., Enfield, D.B., Newman, J.H., 1999. An ~15,000-year record of El Niño-driven alluviation in southwestern Ecuador. *Science* 283 (5401), 516–520.
- Shulmeister, J., 1999. Australasian evidence for Mid-Holocene climate change implies precessional control of Walker Circulation in the Pacific. *Quaternary International* 57/58, 81–91.
- Steig, E.J., Hart, C.P., White, J.W.C., Cunningham, W.L., Davis, M.D., Saltzman, E.S., 1998. Changes in climate, ocean and ice-sheet conditions in the Ross embayment, Antarctica, at 6 ka. *Annals of Glaciology* 27, 305–310.
- Stern, C., 1991. Mid-Holocene Tephra on Tierra del Fuego (54°S) derived from the Hudson Volcano (46°S): evidence for a large explosive eruption. *Revista Geológica de Chile* 18 (2), 139–146.
- Stine, S., Stine, M., 1990. A record from Lake Cardiel of climate in southern South America. *Nature* 345 (6277), 705–708.
- Stuiver, M., Reimer, P.J., 1993. Extended ¹⁴C data base and revised calib 3.0 ¹⁴C age calibration program. *Radiocarbon* 35 (1), 215–230.
- Stuiver, M., Reimer, P.J., Bard, E., Beck, J.W., Burr, G.S., Hughen, K.A., Kromer, B., McCormac, G., Van der Plicht, J., Spurk, M., 1998. INTCAL98 radiocarbon age calibration, 24,000–0 cal BP. *Radiocarbon* 40 (3), 1041–1083.
- Veit, H., 1996. Southern Westerlies during the Holocene deduced from geomorphological and pedological studies in the Norte Chico, northern Chile (27–33°S). *Palaeogeography, Palaeoclimatology, Palaeoecology* 123 (1–4), 107–119.
- Villagran, C., 1988. Expansion of Magellanic Moorland during the Late Pleistocene: palynological evidence from Northern Isla de Chiloé, Chile. *Quaternary Research* 30 (3), 304–314.
- Villagran, C., Varela, J., 1990. Palynological evidence for increased aridity on the Central Chilean Coast during the Holocene. *Quaternary Research* 34 (2), 198–207.
- Walker, M.J.C., Harkness, D.D., 1990. Radiocarbon dating the Devensian Late-Glacial in Britain: new evidence from Llanilid, South Wales. *Journal of Quaternary Science* 5 (2), 135–144.
- Walker, M.J.C., Bryant, C., Coope, G.R., Harkness, D.D., Lowe, J.J., Scott, E.M., 2001. Towards a radiocarbon chronology of the Late-Glacial: sample selection strategies. *Radiocarbon* 43 (2B), 1007–1019.
- Weischet, W., 1985. Climatic constraints for the development of the Far South of Latin America. *GeoJournal* 11 (1), 79–87.
- Xu, S., Zheng, G.D., 2003. Variations in radiocarbon ages of various organic fractions in core sediments from Erhai Lake, SW China. *Geochemical Journal* 37 (1), 135–144.